Computational Structural Engineering
An International Journal
*Vol. 2, No. 1, pp. 25~32 (2002)*

*Computational Structural Engineering Institute*

# Damage Simulation of Natural Draught Cooling Towers

**S.-Y. Noh and Y. Huh†**

*Institute for Structural Statics and Dynamics RWTH Aachen 52056 Aachen, Germany*
*†Department of Civil Engineering The University of Suwon Kyung-Gi, Korea*

Received May 2002; Accepted August 2002

**ABSTRACT**

Natural draught cooling towers often develop visible crack structures as consequences of progressive damage processes over their life-time. The aim of this paper is a numerical demonstration of the progressive damage process of cooling towers, representatively for the reinforced concrete structures, in order to improve the durability and extend the life-time of structures subjected to such damage processes. For the analyses, the applied material model for reinforced concrete will be briefly introduced. An existing natural draught cooling tower with a pronounced crack structure, in which this crack structure indicates the typical damage pattern of large cooling towers will be numerically simulated. The change of dynamical behavior of the structure with regard to natural frequencies, reflecting the global damage process due to the degrading stiffness of the structure in dependence of the load type and intensity, will be presented and discussed.

*Keywords:* cooling tower, global damage process, reinforced concrete, natural frequency, numerical simulation

## 1. Introduction

Natural draught cooling towers occasionally start, after years of apparently crack-free performance, to develop visible meridional cracks which indicate the origin of a damage process. Here the reasons are thermal and hygric effects in the interior of the tower, leading to extensive micro-cracking on the outer face of the shell. These meridional cracks will often propagate and widen markedly as time passes. Such progressive damage processes can be observed worldwide on many large cooling towers, even on recently constructed ones, through modern techniques [9]. They can be also observed on bridges under traffic and on offshore-platforms under sea-wave excitation. The reason for these damage phenomena lies in a dynamic self-adaptation of the structure moving towards higher excitation spectral values, after local initial damage formation: so-called damage-controlled structural self-adaptation [6] which this work will demonstrate with an numerical example.

* Corresponding author
Tel.: +82-031-220-2317; Fax: +82-031-220-2494
E-mail address: huhyoung@mail.suwon.ac.kr

## 2. Structural Damage Indicator

Structural damage processes are always attached to nonlinear responses. The nonlinear matrix equation of motion consists of the following 2nd order implicit matrix differential equation, with $V$ denoting the nodal degrees of freedom, $\dot{V}$ the nodal velocities and $\ddot{V}$ the nodal accelerations.

$$\boldsymbol{M}\cdot\ddot{\boldsymbol{V}}+\boldsymbol{G}(\dot{\boldsymbol{V}},\boldsymbol{V},\boldsymbol{d},t)=\boldsymbol{P}(t) \tag{1}$$

Herein $\boldsymbol{M}$ abbreviates the global mass matrix of the structure. The nonlinear vector functional describes the internal equilibrium due to the forcing process $\boldsymbol{P}(t)$, considering viscous $(\dot{\boldsymbol{V}})$ as well as elastic-plastic actions $(\boldsymbol{V})$ and damage $\boldsymbol{d}$. $t$ denotes physical time. For incremental-iterative techniques (1) can be transformed into a linear differential equation for the increments $\delta\bar{\boldsymbol{V}},\delta\dot{\bar{\boldsymbol{V}}},\delta\ddot{\bar{\boldsymbol{V}}}$ and $\delta\bar{\boldsymbol{P}}$

$$\boldsymbol{M}\cdot\delta\ddot{\bar{\boldsymbol{V}}}\cdot\left.\frac{\partial\boldsymbol{G}}{\partial\dot{\boldsymbol{V}}}\right|_{\bar{V}}\cdot\delta\dot{\bar{\boldsymbol{V}}}+\left.\frac{\partial\boldsymbol{G}}{\partial\boldsymbol{V}}\right|_{\bar{V}}=\delta\bar{\boldsymbol{V}}=\delta\bar{\boldsymbol{P}}=\boldsymbol{P}-\bar{\boldsymbol{P}} \tag{2}$$

From (2) we receive the tangential equation of motion by substituting the equilibrated fundamental state of equa-

tion (1) for $\delta\bar{P}$ and using the abbreviations for tangential damping matrix $C_T$, tangential stiffness matrix $K_T$ and the vector of inertial equilibrium nodal forces $F_I$

$$M \cdot \delta\ddot{\bar{V}} + C_T \cdot \delta\dot{\bar{V}} + K_T \cdot \delta\bar{V} = P - M \cdot \ddot{\bar{V}} - G(\dot{\bar{V}}, \bar{V}, d, t) = P - F_I \tag{3}$$

For the sake of simplicity, we will use in the following the time-independent variant of (3), the so-called tangential stiffness relation.

$$K_T(\bar{V}, d) \cdot \delta\bar{V} = \delta\bar{P} = P - G(\bar{V}, d) \tag{4}$$

Structural damage is generally understood as a stiffness-degradation caused by material deterioration. Therefore damaging effects must be stored in $K_T$, as can be achieved by the application of the multi-scale simulation technique. Information of physical deterioration modeled in constitutive law is homogenized and transferred from the material point level up to the structural level for further use in the main control equations (3, 4). This homogenization technique is presented in [10] for a time-independent response of a shell structure consisting of layered finite elements.

In order to quantify the generated global structural damage, a set of phenomenological damage indicators can obviously be defined from $K_T$ in (3, 4). The most succinct form of damage information in $K_T$ is a set of positive eigenvalues $\lambda_i$ or a set of natural frequencies $f_i$ for the structure under the dynamic actions to be further contemplated. With them the damage indicators are formulated for a discretized structure with $m$ degrees of freedom as

$$D_{fi}(V, d) = 1.00 - \frac{f_i(V, d)}{f_i(V_0, d = 0)}, \quad 1 \le i \le m \tag{5}$$

$D_{fi} = 0$ indicates the undamaged, virgin state $d = 0$. $D_{fi}$ increase with growing damage, interpretable as the quantitative weakness of the structure related to a certain mode shape $i$. Furthermore, in the case of damage-caused failure and loss of structural integrity, they should reach the limit value 1. The second term in equation (5), the deviation of $D_{fi}$ from 1, sometimes addressed as measure of integrity, describes the normalized distance of the structural state from the critical one.

The difficulty in the practical application of these damage indicators is that the number of significant natural frequencies have to be reasonably estimated in advance. This estimation depends however on the type of the structure and its loads. On this account another damage indicator is defined in [11] with only one damage parameter $\tilde{f}_k$. This indicator will be compared with the former indicators $D_{fi}$. The parameter $\tilde{f}_k$ in (7) is based on the deformation increment $\Delta V_k^0$ at the first iteration step of every load increment $k$-the so-called predictor. One obtains $\Delta V_k^0$ from the incremental iteration of the equilibrium of the nonlinear FE-analysis and therefore this doesn't require any additional numerical expense. The damage parameter $\tilde{f}_k$ is obtained by using the RAYLEIGH-QUOTIENT (6) in which the mode shape $\Phi_k$ is substituted by the incremental deformation $\Delta V_k^0$.

$$\tilde{f}_k^2 = \frac{\Delta V_k^{0^T} \cdot K_T \cdot \Delta V_k^0}{\Delta V_k^{0^T} \cdot M \cdot \Delta V_k^0} \tag{6}$$

The damage indicator $D_{\Delta V}$ can be obtained according to the same concept for (5) as

$$D_{\Delta V} = 1 - \frac{\tilde{f}_k}{\tilde{f}_0} \tag{7}$$

with the initial damage parameter $\tilde{f}_0$ calculated for each load case.

## 3. Material Model

Reinforced concrete shows a highly nonlinear material behavior. Its modeling generally requires a multitude of material parameters. Although for realistic numerical analysis of structures the material properties have to be modeled as exactly as possible, the requirements on the precision generally depend on the problem at hand.

For the current work - damage analysis of extremely thin-wall shell structures of big natural draught cooling towers - an adequate simple concrete model in a two dimensional description was used, because the investigated shells primarily fail by tension and the behavior of the reinforcement steels and the bond effect between the cracks determine the failure of the structure. Special attention should be turned therefore on the tension-stiffening model. The model used in the following is described in detail in [14, 15].

### *3.1 Concrete Model*

The applied concrete model is a orthotropic model formulated according to [3] for the biaxial state of stress. Basic advantages of this model description are the compact formulation by the introduction of an equivalent uniaxial strain in the principal stress system and its applicableness on a cyclic load process with only four material

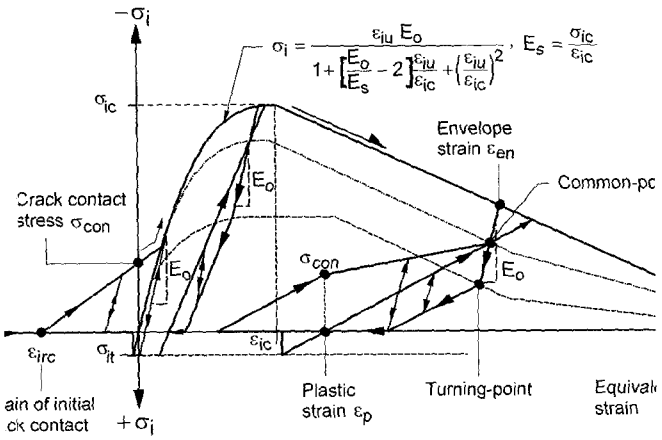


**Fig. 1.** Constitutive law of concrete in principal direction

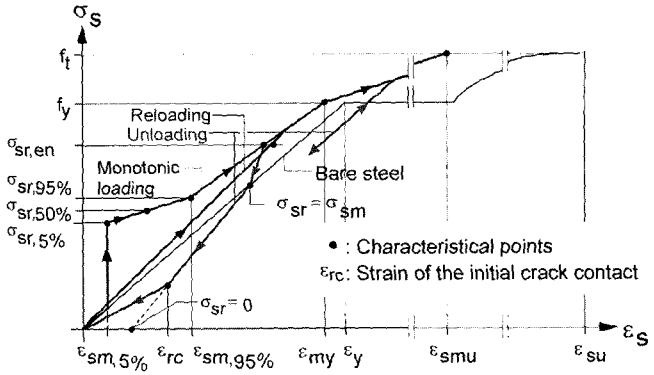


**Fig. 2.** Modified reinforcement law

parameters: tension- and compression strength, strain for the compression strength as well as the initial YOUNG's modulus. The failure criteria are defined based on the experimental results of [13]. The cyclic behavior in compression is formulated based on the experimental data of [7] regarding degradation of strength and stiffness, plastification and energy dissipation.

The principal tensile stress value governs the formation of tension cracking. After tension cracking an uniaxial state is adjusted in the principal stress system. If a tension crack already exists, a second crack may be formed perpendicular to the first one. Depending on the load history and deformation of the structure, the directions of cracks can be rotated according to the principal strain directions and some cracks may close again by local unloading or change of the load direction. For the crack closing process the formulation of [16] are used. The entire model description of the concrete is pictured in Fig. 1.

### *3.2 Modified Reinforcement Model Considering Bond Effect*

The bond effect between concrete and reinforcement plays an important role in the analysis of the response behavior of reinforced concrete structures. For the present investigation the bond effect has to be modeled indirectly as tension-stiffening participation of the concrete between the cracks either in the concrete or in the reinforcement.

In the following the formulation of the tension-stiffening effect assigned to the reinforcement model, is described both for the monotonous and for the unidirectional cyclic loading. For the model set-up the iterative computation concept with a step-by-step integration of [5] was used, which allows the use of any complicated bond law. For monotonous loading the bond model of [12] was employed, which is also valid for large slip e.g. in the case of yielding of the reinforcement. For cyclic loading the bond model of [17] is used because it is more adequate for the service load state compared to other cyclic bond models described in [2]. For efficient computation only characteristic points are determined. The linear connection of these points describes the modified reinforcement model in Fig. 2.

## 4. Progressive Damage of a Cooling Tower Shell

In the numerical analysis the damage evolution in a large cooling tower shell and its spectral shifts under environmental loads were investigated. We choose an existing tower, about 25 years old, with a pronounced crack pattern. Fig. 3 gives the dimensions and an impression of this structure with its varying shell thickness over the height. The cooling tower is characterized by the geometry of the

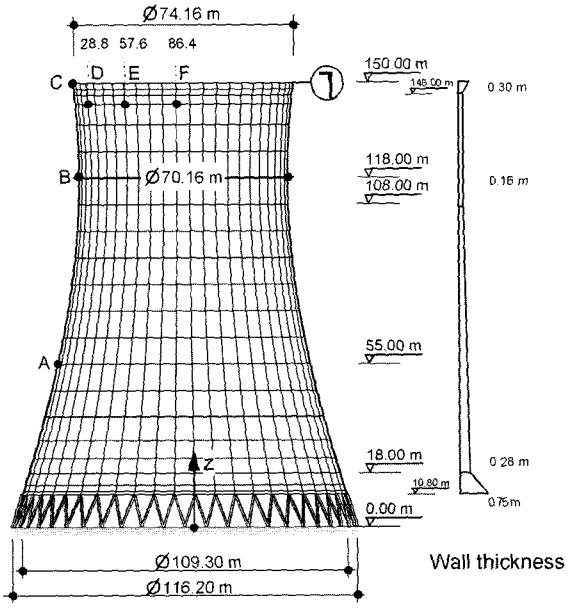


**Fig. 3.** Geometry and wall thickness

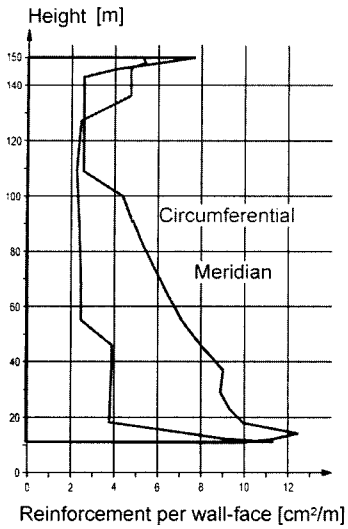


**Fig. 4.** Reinforcement steel

hyperbolic shell described by

$$r(z) = r_0 + \frac{a}{b}\sqrt{b^2 + (H_T - z)^2} \tag{8}$$

with $r_0 = -23.6939\ m$, $a = -58.7739\ m$, $b = 121.6289\ m$ and $H_T = 118.800\ m$.

The top lintel is constructed as a circular ring with $D/B$= 0.30 $m$/1.29 $m$. 50 V-columns with $D/B$ = 0.75 $m$/0.90 $m$ support the shell. Every two columns stand on a foundation ($D/B/H$ = 4.00 $m$/5.00 $m$/1.50 $m$) which is simulated as springs with an assumed WINKLER modulus of $k$ = 12.0 $MN/m^3$.

Fig. 4 portrays the existing reinforcement determined by linear analyses. For the evaluation of the crack width, the diameter of the used reinforcement of 8-12 $mm$ is simplified as 12 $mm$ uniformly. The material data for the used concrete can be found in Table 1. Here the variation coefficient of the tensile strength of the concrete is assumed as 10%. The reinforcement steel is characterized by an initial YOUNG's modulus $E_0 = 210.10^3\ MN/m^2$, a yielding stress $f_y = 410\ MN/m^2$ and a strength $f_y = 460\ MN/m^2$ at a fracture strain of 10%.

The computer simulations use an iso-parametric 4-noded REISSNER-MINDLIN shell element capable of large displacements and large rotations. The displacement shape functions of the element are bilinear polynomials, and to avoid shear-locking the transverse shear strains are linearly interpolated in the sense of an assumed strain element. The incremental-iterative solution of the structural response up to failure has followed the multi-scale analysis technique, using the FEMAS-software [1]. The complete structure is modeled as a layered shell continuum consisting of 2 orthogonal uniaxial steel layers on both faces and 9 plane stress concrete layers.

**Table 1.** Concrete data

| Component | Concrete | $\beta_{W28}$ [MN/m³] | $\beta_{cm}$ [MN/m³] | YOUNG's modulus [MN/§³] |
|---|---|---|---|---|
| Shell | BH300 | 25.0 | 2.675 | 30000 |
| Support | BH450 | 40.0 | 2.924 | 35500 |
| foundation | BH300 | 25.0 | 2.675 | 30000 |

The tower is subjected to actions from its dead weight $G$, quasi-static wind load of wind $W$ zone I with K1.0 according to [18] and alternatively to temperature loads due to winter service condition, a temperature difference of 45 K from the cooler outer to the warmer inner part. In addition the hygric effect of permanent wetting on the inner face and the shrinkage on the outer face are considered as a temperature load. A reasonable assumption according to [4] results in an equivalent temperature gradient of 15 K for a nearly 30 years old tower.

Fig. 5 and 6 illustrate comparatively the load-deflection curves at the investigated points B and E in Fig. 3 for the

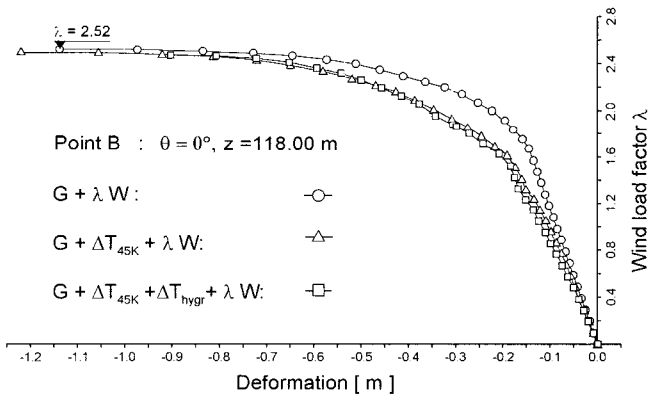


**Fig. 5.** Load deflection curves at point B

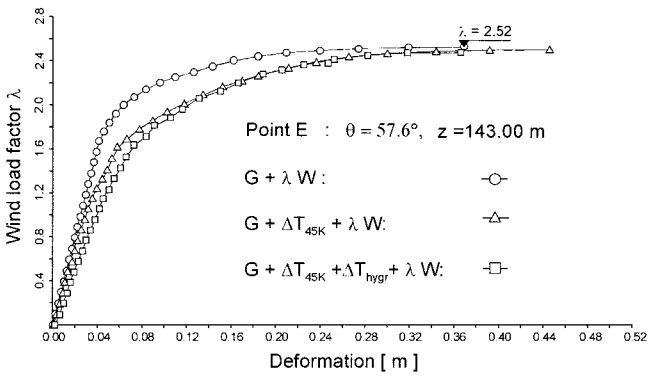


**Fig. 6.** Load-deflection curves at point E

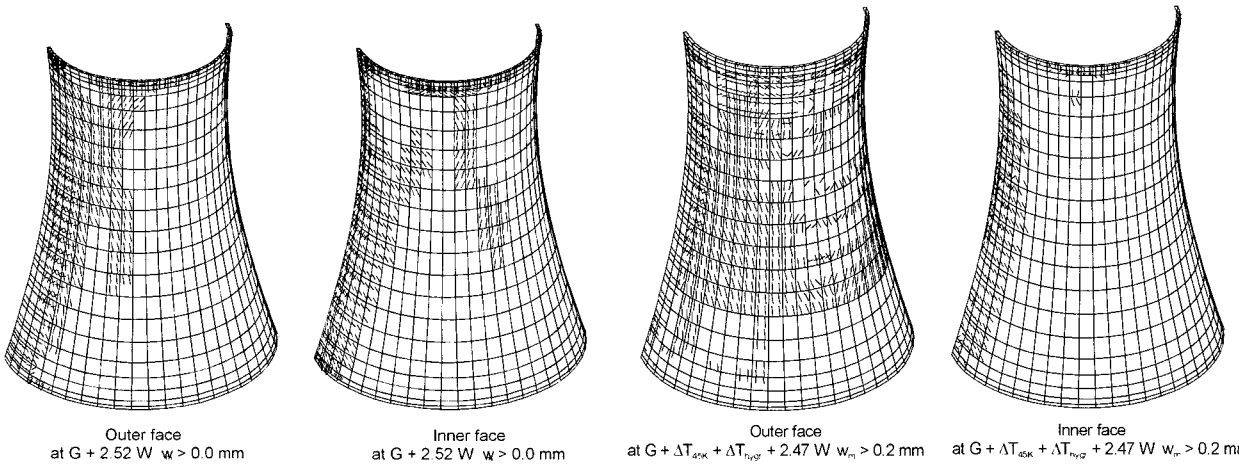


**Fig. 7.** Crack patterns under G+2.52W and $G+\Delta T_{45K}+\Delta T_{hygr}+$ 2.47W.

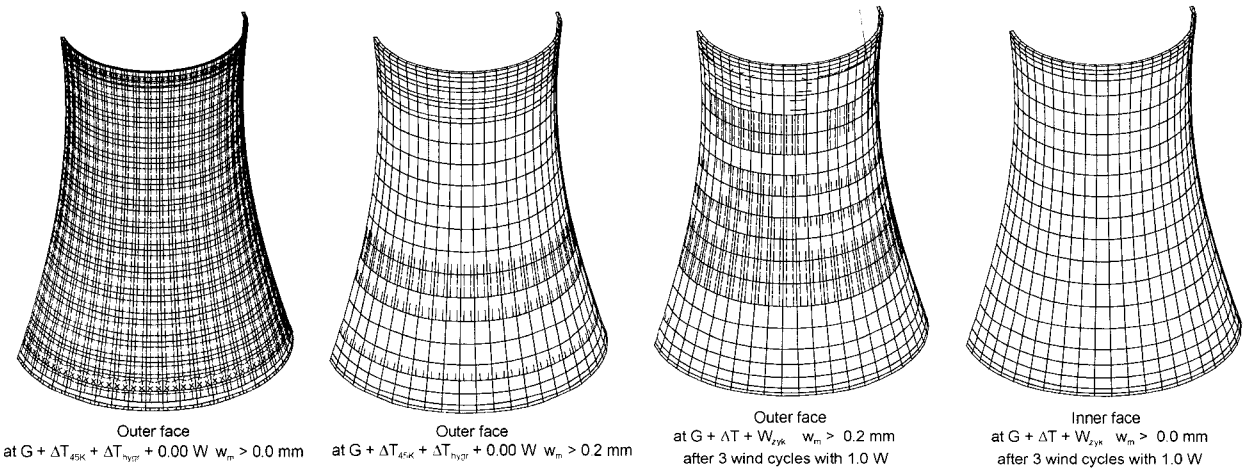


**Fig. 8.** Crack patterns under $G+\Delta T_{45K}+\Delta T_{hygr}$+0.00W, $G+\Delta T+W_{zyk}$ and after 3×1.0W wind cycles

three load cases. The crack pattern close to the collapse state is pictured in Fig. 7. Without thermal service loads the shell behaves linearly up to a wind load factor $\lambda = 1.75$. After this load level, cracks form and develop horizontally on the luff side as well as vertically on the flank, successively. They propagate and join together with increasing wind load. Compared to that, the temperature load $\Delta T_{45K}$ under winter service condition forms cracks on the whole outer face of the shell. The hygric effect increases the grade of this initial damage, leading particularly to circumferential bending damage in the area of the flank. This initial damage tends however to be reduced with increasing wind load factor and finally the wind load alone determines the collapse behavior of the tower. Thus the tower collapses approximately at the same wind load factor of $\lambda \approx 2.50$ under all the investigated load cases.

In Fig. 8 on the right the crack patterns of the shell after 3 consecutive cyclic wind loads 1.0 W are plotted. Here the tower has been already loaded first by the winter service temperature difference $\Delta T_{45K}$ and the hygric effect $\Delta T_{hygr}$ and subsequently unloaded to a decreased normal service temperature of $\Delta T_{25K}$.

Comparing with the crack patterns before the loading of cyclic winds in Fig. 8 on the left, one can see the increase of the cracks due to the cyclic wind excitation. This crack pattern obtained from the numerical analysis describes qualitatively the existing real damage state of the tower. The definitely insufficient existing circumferential amount of reinforcement is responsible for the pronounced damage of the tower. The average reinforcement in the circumferential direction of the shell is 0.25%, while [18] recommends 0.3%-0.4%

As discussed in Section 2, the influence of stiffness reduction in the wake of the damage process from the above quasi-static analyses has to be identified by the shift of the natural frequencies. Fig. 9 shows the shift of the first 3 natural frequencies over the wind load factor $\lambda$, comparing the load cases with and without initial damage.

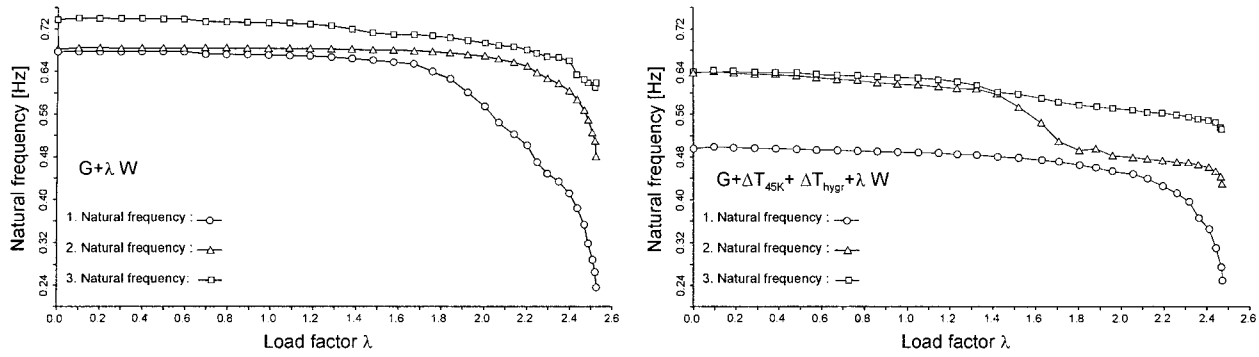


**Fig. 9.** Shift of the first 3 natural frequencies as a function of wind load factor $\lambda$

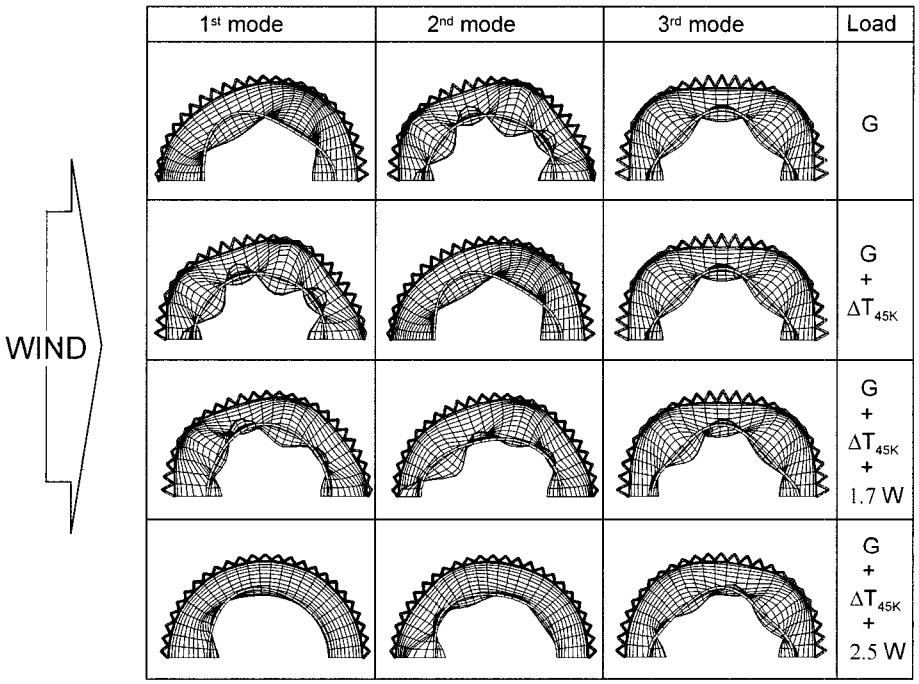


**Fig. 10.** Shift of the first 3 natural modes under $G+\Delta T_{45K}+\lambda W$

Under the load combination $G+\lambda W$ the 3 natural frequencies between $f = 0.67$ Hz and $f = 0.74$ Hz remain approximately constant up to the occurrence of the successive formation of horizontal cracks on the luff at $\lambda = 1.75$. Afterwards the first one varies dramatically until the collapse of the tower, whereas both other remain nearly constant for much longer. The reduction of the stiffness due to temperature and hygric swelling decreases the natural frequencies. The first one shifts e.g. from 0.67 Hz and 0.49 Hz, this is nearly 30% reduction. Under the load combination $G+\Delta T_{45K}+\Delta T_{hygr}+\lambda W$, one can see, in comparison to the former case, the more sensitive behavior of the second natural frequency over the wind load: the whole structure has been already so strongly damaged by temperature and hygric effects that the local damage increase under the low wind load cannot change the first natural frequency remarkably. It apparently varies only under a higher level of wind loads.

The shifted natural modes of the investigated damage states in Fig. 10 indicate the changing dynamic properties of the structure in detail. The undamaged tower has its first three natural modes with 3, 5 and 4 waves respectively. However, after the formation of cracks on the whole outer face of the tower due to the temperature load, the new first mode with a natural frequency of $f = 0.58$ *Hz* now has 5 waves, like the 2nd original mode. At the wind load level $\lambda = 1.70$ at which the second natural frequency drops sharply, the second mode has 5 waves. From this load level onwards the first mode is quite similar to the real-life deformed figure of the structure. At a load level close to collapse ($\lambda = 2.50$), the second mode also assumes a similar form to the deformation of the structure. The eval-

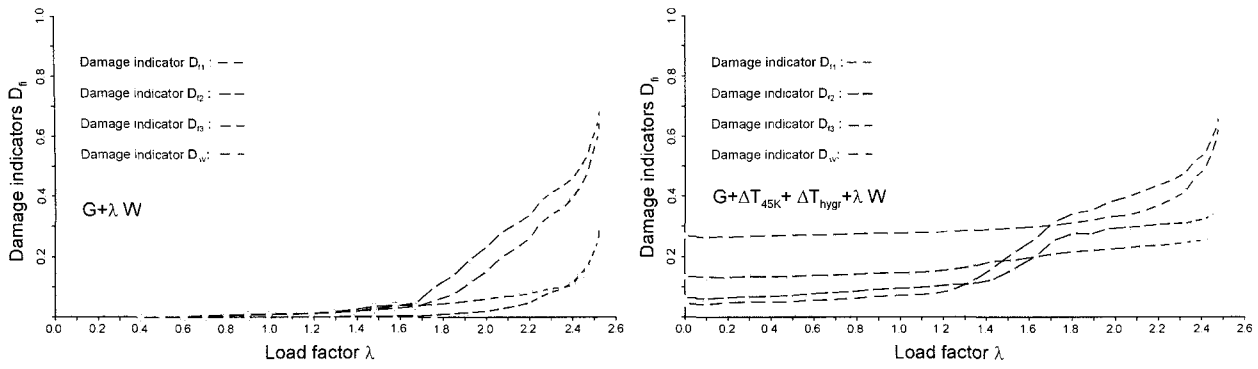


**Fig. 11.** Damage indicators $D_{f1}$, $D_{f2}$, $D_{f3}$ and $D_{\Delta V}$

uations of natural frequencies and natural modes under consideration of the hygric effect (reported in [14]) show in principle the same behaviour.

The damage indicators $D_{fi}$ based on the natural frequencies in Fig. 11 reflect these damage processes effectively as expected. Under both load combinations $G+\lambda W$ and $G+\Delta T_{45K}+\Delta T_{hygr}+\lambda W$, $D_{f1}$, $D_{\Delta V}$ faithfully mirrors the global damage state of the cooling tower. Compared to $D_{f1}$, $D_{\Delta V}$ indicates the damage process induced by the currently applied wind loads. Wind loads of lower intensity than $\lambda$=1.75 damage only local bounded areas of the shell. Therefore the values of $D_{\Delta V}$ remain under the global damage values of $D_{f1}$ and the curve for $D_{\Delta V}$ is similar to the one for $D_{f2}$. After the wind load level $\lambda$ = 1.75 is reached, the damage process due to wind dominates the global damage state of the shell and $D_{\Delta V}$ corresponds with $D_{f1}$. The application of both indicators allows the identification of the global damage state as well as damage process in local areas.

Additional damage indicators based on natural frequencies make it possible to estimate the increase of wind excitation level due to damage formation without time-consuming nonlinear analyses. In Fig. 12 the first natural frequencies for some load cases are plotted into the VON-KÁRMÁN-spectrum. In the standard spectrum, $S$ denotes the spectral density function of the wind excitation, $f$ the respective excitation frequencies and $\sigma$ the variance. The figure clearly demonstrates the wind- and temperature-induced shifts of the first natural frequencies from their virgin positions towards the spectral peak. It is noticeable that the temperature and the hygric effect alone increase the dynamic excitation levels about 10% and 25%. Without any further nonlinear dynamic computations one can thus deduce from the increase of the spectral excitation level to an approximately equally large increase of the internal stresses in regard to the first damaged mode shape.

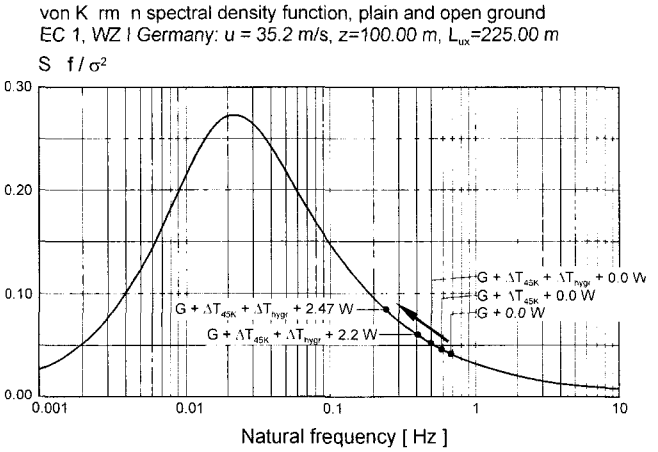


**Fig. 12.** Damage induced increase of wind dynamics

## 5. Conclusions

In this paper progressive damage processes of natural draught cooling towers were demonstrated. Such damage processes have been recently also observed on different kinds of structures. The common features of the damage process are the wide-band excitation, a shift of the structural response spectrum towards higher excitation caused by degrading structural stiffness, as well as a damage-controlled self-adaptation phenomenon. The damage processes develop progressively over the life-time of the structures. Therefore they have to be considered in the design phase through a durability oriented design, which take into account the changing structural response under deterioration and damage processes- a restoration is usually difficult; maintenance and repair costs may become substantial.

## References

**Beem H, Könke C, Montag U, Zahlten W** (1996) FEMAS 2000 -

Finite element modules of arbitrary structures, Institute for Statics & Dynamics, Ruhr-University Bochum, Users Manual Release 3.0.

**CEB 210** (1991), Behavior and analysis of Reinforced concrete structures under alternate actions inducing inelastic response-volume 1, CEB Bulletin d'Information 210, Comité Euro-International du Béton, Lausanne.

**Darwin D, Pecknold DA** (1977) Nonlinear biaxial stress-strain law for concrete, Journal of the Engineering Mechanics Division, 103(EM2): 229-241.

**DIN 4227** (1988) Spannbeton.

**Eligehausen R, Popov EP, Bertero VV** (1983) Local bond stress-slip relationships of deformed bars under generalized excitations, College of engineering, University of California.

**Harte R, Krätzig WB, Noh S-Y, Petryna YS** (2000) On progressive damage phenomena of structures, Computational Mechanics, 25: 404-412.

**Karsan ID, Jirsa JO** (1969) Behavior of concrete under compressive loadings, Journal of the Structural Division, ASCE, 95(ST12): 2543-22563.

**Krätzig WB, Gruber K, Zahlten W** (1992) Numerical collapses simulations of large cooling towers, tech. report No. 92-3, Institute for Statics & Dynamics, Ruhr-University Bochum.

**Krätzig WB, Gruber K** (1992). Large-cycle damage simulations of natural draught cooling towers, The 4th Int. Symposium on Natural Draught Cooling Towers, 151-158, Kaiserslautern, Germany.

**Krätzig WB** (1997) Multi-level modeling techniques for elasto-plastic structural responses, in D.R.J. Owen et al., editors, Computational Plasticity, pages Part 1, 457-468. CIMNE-Int. Center for Num. Meth. in Engng., Barcelona.

**Krätzig WB, Noh SY, Chen F** (2000) Theorie und Simulation progressiver Schädigungsprozesse von Naturzugkühltürmen unter Wind- und Temperatureinwirkungen. Abschußbericht des DFG-Forschungsprojektes.

**Kreller H** (1990) Zum nichtlinearen Trag- und Verformungsverhalten von Stahltbetonstabtragwerken unter Last- und Zwangeinwirkung, Heft 409, Deutscher Ausschuß für Stahlbeton.

**Kupfer H, Hilsdorf HK, Rüsch H** (1969) Behavior of concrete under biaxial stresses, ACI Journal, 66(8): 656-666.

**Noh SY** (2001) Beitrag zur numerischen Analyse der Schädigungsmechanismen von Naturzugkühltürmen, Dr.-Ing. Thesis, RWTH, Department of Civil Engineering, Aachen, Germany.

**Noh SY, Krätzig WB, Meskouris M** (2002) Numerical simulation of serviceability, damage evolution and failure of reinforced concrete shells, In Press in Computers & Structures.

**Su X, Zhu B** (1994) Algorithm for hysteresis analysis of prestressed-concrete frames, Journal of Structural Engineering, 120(6): 1732-1744.

**Tue NV** (1993) Zur Spannungsumlagerung im Spannbeton bei der Rißbildung unter statischer und wiederholter Belastung, Heft 435, Deutscher Ausschuß für Stahlbeton.

**VGB-BTR** (1997) Guideline: Structural Design of Cooling Towers, Essen.